MATERIALS CHEMISTRY
FRONTIERS

CHINESE CHEMICAL SOCIETY

ROYAL SOCIETY OF CHEMISTRY

RESEARCH ARTICLE

View Article Online
View Journal | View Issue

Cite this: *Mater. Chem. Front.*, 2021, **5**, 1315

Boosting the ionic conductivity of PEO electrolytes by waste eggshell-derived fillers for high-performance solid lithium/sodium batteries†

Laiqiang Xu,[a] Jiayang Li,[a] Wentao Deng,[a] Lin Li,[a] Guoqiang Zou,[a] Hongshuai Hou,[a] Lanping Huang*[b] and Xiaobo Ji*[a]

Poly(ethylene oxide) (PEO)-based polymer electrolytes are extensively investigated, and they have rapidly developed in all-solid-state batteries (ASSBs) over recent years for their good interface contact with electrodes, easy shaping and decent flexibility. However, their low ionic conductivity remains a serious issue to be solved urgently. Researchers have found that the addition of fillers can improve the ionic conductivity *via* creating more amorphous regions conducive to ion transport in PEO. Here, we adopted waste eggshell as a precursor to prepare a sub-micron filler, which is mainly CaO, and it was added into the PEO electrolyte to get a composite polymer electrolyte. Close contact *via* Lewis base-acid interaction between CaO and PEO can be obtained, as CaO is an effective filler with strong alkalinity. To the best of our knowledge, this is the first time it is applied in the PEO electrolyte. The filler significantly decreases the crystallinity of PEO, and hence, boosted ionic conductivity of the composite polymer electrolyte is observed, which is about 4.5 times higher than that of the polymer reference electrolyte. It additionally brings a higher tensile strength along with a more stable electrochemical window (up to 5 V) to the composite electrolyte. Therefore, as expected, the all-solid-state Li/Na battery with this composite electrolyte exhibits long cycling life and excellent rate performances. The corresponding Li/$LiFeO_4$ battery has a stable capacity of 142.8 mA h g^{-1} at 1C after 200 cycles, and the corresponding solid-state Na/$Na_3V_2(PO_4)_3$ battery gives a reversible capacity of 101.2 mA h g^{-1} at 0.5C after 100 cycles.

Received 27th July 2020,
Accepted 16th August 2020

DOI: 10.1039/d0qm00541j

rsc.li/frontiers-materials

1. Introduction

Conventional lithium/sodium-ion secondary batteries based on liquid electrolytes have been vastly developed in recent years,[1–4] yet disadvantages such as unsafety, liquid leakage, uncontrollable side reactions and dendrite issues seriously limit their further development.[5–8] All-solid-state batteries (ASSBs), the batteries with all parts solid including the electrolyte, can provide effective solutions to those practical problems.[9–11] Particularly, the solid electrolyte, as a key part in ASSBs, plays a vital role in facing the challenges of traditional batteries. It includes inorganic electrolytes and polymer electrolytes. Though some inorganic solid electrolytes own the ionic conductivities comparable to that of liquid electrolytes,[12–15] towards practical application in full batteries, the interface and mechanical rigidity concerns are hard to overcome.[16–18] In comparison with the inorganic electrolyte, the solid polymer electrolyte is more promising for the advantages of compatibility with electrode materials, good flexibility, easy shaping and cost-effectiveness.[19,20]

Polyethylene oxide (PEO)-based electrolytes are the most extensively utilized polymer solid electrolytes.[21–23] The other frequently used polymer electrolytes include polyacrylonitrile (PAN),[24] polyvinylidene fluoride (PVDF)[25] and polymethyl methacrylate (PMMA).[26] However, similar to other polymer electrolytes, PEO electrolytes suffer from low ionic conductivity, which is $\sim 10^{-7}$ S cm^{-1} at room temperature.[27] Various strategies involving addition of liquid plasticizers,[28] construction of block copolymers[29] and introduction of fillers[30] have been applied to improve the ionic conductivity. Introducing fillers to get a composite electrolyte can obviously improve the ionic conductivity without sacrificing the thermal stability or electrochemical stability. For instance, research on Al_2O_3,[31] SiO_2,[32] TiO_2,[33] and ZrO_2[34] has reported enhancement in the ionic conductivity of polymer electrolytes by increasing the amorphous region of the polymer, which promotes the lithium ion transport. Recently, Luo group has reported that vertically

[a] College of Chemistry and Chemical Engineering, Central South University, Changsha, 410083, China. E-mail: christie@mail.csu.edu.cn, xji@csu.edu.cn; Tel: +86 731-88877237
[b] Science and Technology on High Strength Structural Materials Laboratory, Central South University, Changsha, 410083, China

† Electronic supplementary information (ESI) available. See DOI: 10.1039/d0qm00541j

aligned vermiculite sheets (VAVSs) could be applied as fillers.[35] Its corresponding composite electrolyte can provide continuous paths for Li^+ transport at the interface. The ionic conductivity and Li^+ transference number were enhanced by the addition of the VAVS. Li *et al.* synthesized a composite electrolyte by incorporating MnO_2 nanosheets with PEO.[36] The MnO_2/PEO electrolyte exhibited an ionic conductivity of 1.95×10^{-5} S cm^{-1} at 30 °C, while it is only 1.38×10^{-5} S cm^{-1} for the pure PEO. Apart from the conductivity, better tensile strength was observed in the composite electrolyte.

Despite the above-mentioned progress, the effect of inorganic fillers on increasing the amorphous region of polymers and improving the transport of ions is limited because of the insufficient interaction between the fillers and polymer chains. In addition, the complex synthesis process for constructing effective nanoscale inorganic fillers is an obstacle to obtain high-ionic-conductivity electrolytes. Compared with the common metallic oxide filler, CaO with a stronger alkalinity can more efficiently destroy the crystalline area of the polymer electrolyte, realizing a composite electrolyte with high ionic conductivity. As the main component of the waste eggshell is calcium carbonate, it is facile to obtain a CaO-based filler using the waste eggshell as the precursor. At the same time, it is an environment-friendly strategy, as it is a waste utilization approach.

In this work, we put forward a novel inorganic filler derived from eggshell (FDE). Since eggshell is mainly $CaCO_3$, the filler obtained by first ball-milling and then calcination of the eggshell is almost CaO. This is the first time that CaO is applied as a filler for a composite electrolyte. CaO is a lithiophilic material, and it can adsorb/desorb Li^+/Na^+ on the surface to promote the diffusion. This filler shows superior ionic conductivity, which we propose is from its stronger alkalinity than that of the other inorganic fillers and its mixed ingredients derived from multiple components of the eggshell. The pair of factors has a synergetic effect on the PEO polymer chain, making the filler-based electrolyte deliver a higher ionic conductivity than the composite electrolyte with commercial CaO. The ionic conductivity of the FDE-based Li^+ polymer electrolyte (a mix of FDE, PEO and $LiClO_4$) can reach 6.39×10^{-5} S cm^{-1} at ambient temperature, much higher than that of the FDE-free Li^+ polymer electrolyte (7.06×10^{-6} S cm^{-1}). Meanwhile, the FDE-based Na^+ polymer electrolyte (a mix of FDE, PEO and $NaClO_4$) achieves an ionic conductivity of 4.9×10^{-5} S cm^{-1} at room temperature. With the addition of FDE, the whole amorphous regions of the PEO polymer are increased, and the tensile strength and electrochemical stability windows are improved. As expected, the all-solid-state Li/$LiFeO_4$, Na/$Na_3V_2(PO_4)_3$ batteries based on composite electrolytes display outstanding cycling stabilities and rate performances.

2. Experimental section

Preparation of FDE materials

Chicken eggshell was collected from the local market, Changsha, Hunan province of China. The eggshell was washed several times with deionized water aiming at getting rid of impurities. After that, the pretreated eggshell was dried at 60 °C overnight. Then, the eggshell was subjected to ball-milling treatment at 500 rpm for 12 h to get uniform eggshell bits. At last, calcination of eggshell bits was conducted in a muffle oven at 1000 °C for 2 h to get the filler.

Preparation of composite polymer electrolytes

Polyethylene oxide (PEO, Sigma-Aldrich), lithium perchlorate ($LiClO_4$, 99.99%, Aladdin), and sodium perchlorate ($NaClO_4$, 99.99%, Aladdin) were dried in a vacuum oven at 50 °C for 24 h before use. A solution casting technique was applied to prepare composite electrolytes. PEO, $LiClO_4$ (or $NaClO_4$), and FDE material were mixed in acetonitrile (CH_3CN, AR grade) and stirred for 12 h to obtain a homogenous suspension (nEO : nLi/Na = 20 : 1). Then the suspension was casted on a polytetrafluoroethylene (PTFE) plate and dried at 80 °C under vacuum for 24 h to get composite polymer electrolytes (CPEs) with a thickness of ~90 μm. For comparison, the polymer electrolyte without inorganic fillers was prepared by the same method. All the solid electrolyte films were placed in an argon-filled glove box before testing.

Material characterization

A field-emission scanning electron microscope (FESEM, JSM-7001F) was used to observe the structure of the eggshell and the derived filler. X-ray diffraction (XRD, Rigaku Model ULTIMA IV, CuKα radiation) and inductively coupled plasma mass spectrometry (ICP-MS, Agilent 7800ce) were employed to investigate the structure and composition of the sample. FTIR spectra were recorded in the frequency range of 400–4000 cm^{-1} using an FTIR spectrophotometer (Jasco, FT/IR-4100, Japan). Thermogravimetric analysis (TGA, STA2500) and differential scanning calorimetry (DSC, NETZSCH DSC 200PC) were carried out in a N_2 atmosphere at a temperature ramp of 10 °C min^{-1}. The particle size of final FDE materials was determined using a Winner802 DLS Photon correlation nano particle size analyzer. The mechanical properties of the composite polymer electrolyte film were analysed using an MTS Insight machine (23 MTS Insight). A three-dimensional video microscope (KH-7700, HIROX) was used to observe the crystal particle of the composite electrolyte.

Electrochemical measurements

The ionic conductivity of the composite polymer electrolyte was calculated using the equation ($\sigma = L/R_bS$), where L is the thickness of the polymer electrolyte film, R_b is the electrolyte resistance calculated from the blocking stainless steel electrode by electrochemical impedance spectroscopy, and S stands for the surface area of the electrolyte film. The electrolyte resistance was obtained by electrochemical impedance spectroscopic testing of symmetric blocking cells using a PARSTAR 2273 in the a frequency range from 200 kHz to 0.1 Hz. The electrochemical window of the composite electrolyte was determined by linear sweep voltammetry of the stainless steel/CPE/Li or stainless steel/CPE/Na battery.

For full-cell performance test, $LiFeO_4$ (Hefei Kejing Materials Technology Co., Ltd)/$Na_3V_2(PO_4)_3$ (reported in our previous work) was the active material.[3] The working electrode included 70.0 wt% of active materials ($LiFeO_4$ or $Na_3V_2(PO_4)_3$), 15.0 wt% of conductivity agent (acetylene black) and 15.0 wt% of binder (polyvinylidene difluoride, PVDF). The mixed materials in *N*-methyl-2-pyrrolidone (NMP) were spread on the aluminum foil, and then dried at 100 °C under vacuum for 12 h. Metallic lithium or sodium were applied as the reference electrode. The full cells were assembled in an argon-filled glove box. A LAND-CT2001C test system was used for the electrochemical measurement.

3. Results and discussion

The samples were characterized by XRD, as shown in Fig. 1a. The XRD pattern of the eggshell shows the same diffraction pattern as $Mg_{0.03}Ca_{0.97}CO_3$ (JCPDS no. 89-1304), indicating that the eggshell is mainly composed of $CaCO_3$ and $MgCO_3$. After being calcined at different temperatures (700 °C, 800 °C, 900 °C, and 1000 °C) to investigate the most appropriate calcination temperature, the eggshell was eventually calcined at 1000 °C to prepare the filler. As depicted by XRD patterns in Fig. 1a, at 700 °C, the calcined eggshell has obvious peaks of residual $CaCO_3$. As the temperature raised to 800 °C, the diffraction peaks of $CaCO_3$ disappeared, implying that the $CaCO_3$ in eggshell was fully decomposed.

Distinct peaks of CaO (JCPDS no. 77-2010) for the calcined eggshell at 1000 °C appeared at at 32.2°, 37.3°, 53.8°, 64.1°, 67.4°, and 79.6° corresponding to the (111), (200), (220), (311), (222) and (400) lattice planes. The results can be further confirmed by TG analysis. As demonstrated in Fig. 1b, the eggshell has an endothermic reaction at 727.7 °C. Therefore, for the following eggshell precursors, they were calcined at 1000 °C to assure complete conversion of $Mg_{0.03}Ca_{0.97}CO_3$. Fig. 1c and Table S1 (ESI†) list the composition of this sample, which was determined by ICP, and it shows that the calcined eggshell mainly consists of CaO and MgO. This multiple-component property of the filler can provide a synergetic effect on the polymer chain, leading to a higher ionic conductivity. Additionally, the XRD technology was utilized to explore the crystal structure change of PEO after the addition of the FDE filler. As depicted in Fig. 1d, PEO has two obvious diffraction peaks at 19.0° and 23.2°. No phase change occurs after the introduction of the FDE filler. However, the diffraction peaks become weaker and broader, demonstrating the decrease in the crystallinity of $LiClO_4$/$NaClO_4$-based PEO composite electrolytes, which are ascribed to the Lewis acid–base interactions caused by the PEO electrolyte and filler. The decreased crystallinity of PEO is beneficial for increasing its ionic conductivity, as the amorphous regions of the PEO electrolyte are effective to enhance the ionic conductivity.[13] Therefore, the performance of the composite electrolyte is expected to be enhanced.

The SEM technique was applied to look into the structure of the eggshell and the corresponding filler. Fig. 2a displays the initial morphology of the eggshell, which shows a few large chunks. It is a common morphology of the eggshell (*i.e.* a whole piece including some pores on the surface). In order to even the size of the final product, the ball-milling technique was employed to crush the large pieces and smash all particles. It can be seen that the whole structure of the eggshell is destroyed and particles become more uniform in size after ball-milling (Fig. 2b). Therefore, the corresponding filler is mainly composed of 220 nm and 260 nm size particles (Fig. 2c and d), which was confirmed using a nanoparticle size analyzer. In contrast, when not treated by ball-milling, the obtained filler consisted of aggregated micro-size particles, as shown in Fig. S1 (ESI†), which is not favorable for ion transport.[48] In general, micro-size fillers will increase the blocking effect, which is not favorable for ion transfer, and the decrease in the particle size can mitigate the blocking. The FDE from the eggshell treated by ball-milling

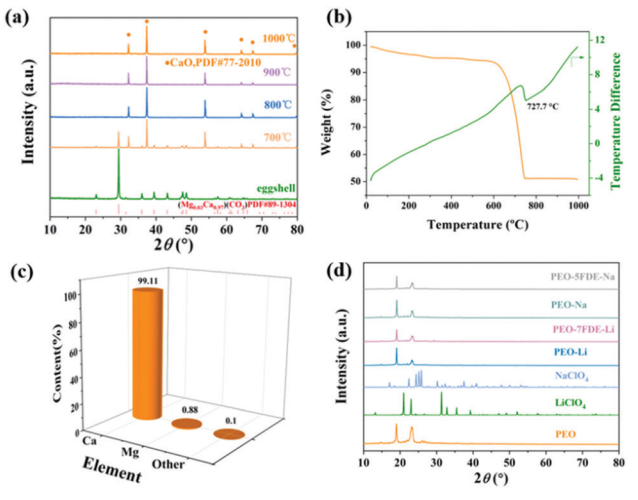

Fig. 1 (a) XRD patterns of uncalcined and calcined eggshell at 700, 800, 900, and 1000 °C. (b) TG and DTA curve of eggshell. (c) ICP data of calcined eggshell at 1000 °C. (d) XRD patterns of each component and the corresponding composite electrolytes.

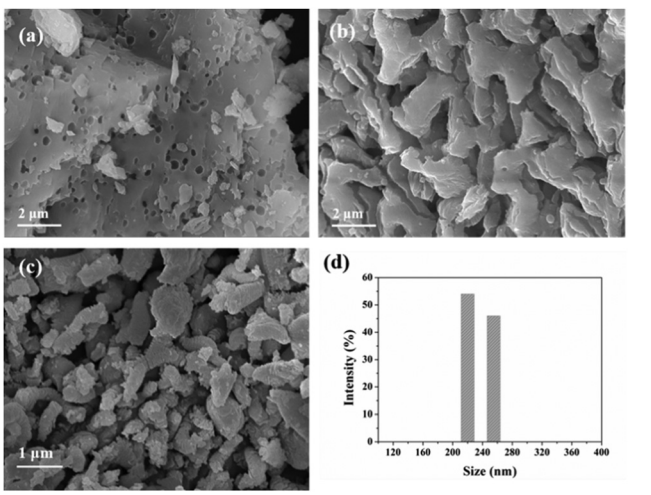

Fig. 2 SEM pattern of (a) untreated eggshell, (b) ball-milling-treated eggshell, and (c) calcined eggshell. (d) Size distribution of calcined eggshell obtained using a nanoparticle size analyzer.

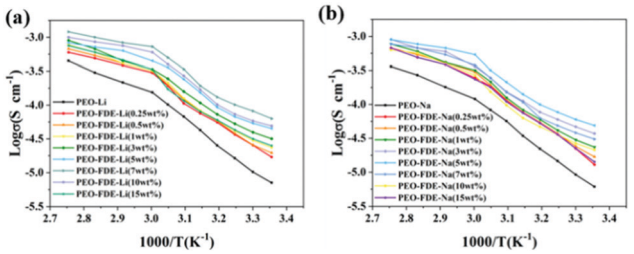

Fig. 3 Temperature-dependent ionic conductivity of (a) PEO–FDE–Li and (b) PEO–FDE–Na with different FDE contents.

demonstrates a decreased particle size, and thus, it could effectively avoid the blocking effect and bestow the polymer electrolyte with a better ionic conductivity.[37,38] Moreover, samples with tiny particles possess a large specific surface area, causing a more significant effect on destroying the crystalline area of PEO.

The ionic conductivity related to the ability of Li^+/Na^+ transport is crucial to a polymer electrolyte, which has a great influence on the electrochemical performance of a full cell. In Fig. 3, the temperature-dependent ionic conductivities of the composite electrolyte with different FDE contents are shown in detail. It was found that with the addition of FDE, the ionic conductivity of polymer electrolyte is enhanced, which is ascribed to the decrease in the crystalline region of PEO. As the increase in the amorphous region leads to enhanced segmental motion, the ionic conductivity is correspondingly improved. A further increase in the filler content will result in a decrease in the ionic conductivity, owing to the aggregation of the filler. Compared with the FDE-free polymer electrolyte, all the FDE-based composite polymer electrolytes show an obvious increment in the ionic conductivity due to the improved polymer chain segment mobility.[39] The comparison of the ionic conductivity of the FDE-based composite electrolyte and the FDE-free electrolyte is discussed in Table S2 (ESI†). For the Li^+ system, the optimal ionic conductivity reaches 6.39×10^{-5} S cm^{-1} (25 °C), which belongs to the PEO–FDE–Li composite electrolyte with 7 wt% FDE filler (PEO–7FDE–Li). At the same time, the PEO–FDE–Na composite electrolyte with 5 wt% FDE (PEO–5FDE–Na) shows a maximum ionic conductivity of 4.9×10^{-5} S cm^{-1} (25 °C). Moreover, the composite polymer electrolyte with commercial CaO was also investigated. In the same ratio, the FDE-based composite electrolytes possess a higher ionic conductivity than that of the commercial CaO-based electrolyte (Fig. S2, ESI†), which are all higher than that of the pure PEO electrolyte. The sub-micron size and the synergetic effect of multicomponents are the main reason that FDE composite electrolyte can have a better function.[40] As observed in the Fig. S3 (ESI†), commercial CaO consists of micron-size particles, which is not conducive to ion transmission. Furthermore, commercial CaO has a much lower specific surface area (2.83 m^2 g^{-1}) than the FDE (19.09 m^2 g^{-1}) (Fig. S4, ESI†), which is inferior in destroying the crystallinity of PEO.

A microscope was used to directly observe the crystallization behavior of the polymer electrolyte after the addition of FDE (shown in Fig. 4). When FDE was introduced, the polymer crystal was different from that observed before (Fig. 4b and d). Yellow circles represent the spherocrystal of the PEO electrolyte. The crystal size was decreased and a larger amorphous region was formed, which explained the increase in the ionic conductivity. TG and DTA measurements were further employed to characterize the crystallization variation of electrolytes. Compared with FDE-free PEO–Li or PEO–Na polymer electrolytes, PEO–7FDE–Li and PEO–5FDE–Li indicate lower melting temperatures, as shown in Fig. 5a and b, which is assigned to the decreased polymer crystallization. At the same time, the thermostability of the composite electrolytes is improved upon introducing the FDE. It can be addressed to eliminating the risk of thermal runaway under extreme conditions.[41] In addition, the DSC measurement was applied to observe the crystalline change caused by the FDE filler.[42] As displayed in Fig. 5c and d, the endothermic peak temperatures of PEO–Li/PEO–Na are higher than those of the composite polymer electrolyte, which is in agreement with the DTA curves. As listed in Table 1, the enthalpy of melting (ΔH_m) and crystallinity (χ_c) were calculated

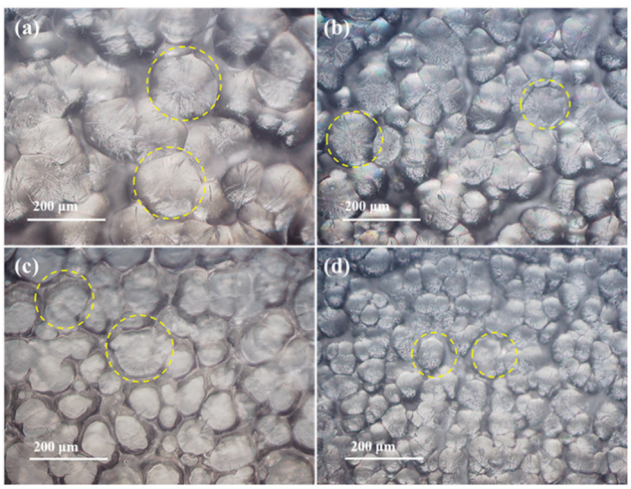

Fig. 4 Microscope images of (a) PEO–Li, (b) PEO–7FDE–Li, (c) PEO–Na, and (d) PEO–5FDE–Na.

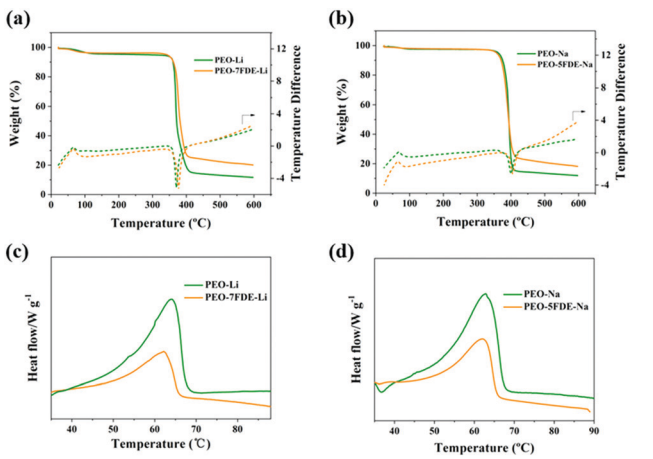

Fig. 5 TG and DTA (a and b) and DSC (c and d) curves of PEO–Li, PEO–7FDE–Li, PEO–Na, and PEO–5FDE–Na.

Table 1 DSC data for the PEO–FDE composite electrolyte

Sample	T_m/°C	ΔH_m/J g^{-1}	χ_c (%)
PEO–Li	64.09	154.08	78.97
PEO–7FDE–Li	62.17	82.56	42.34
PEO–Na	62.76	108.84	55.82
PEO–5FDE–Na	61.58	67.32	34.52

to verify the changes in the polymer electrolyte.[43] In comparison with the pure PEO–Li and PEO–Na, composite electrolytes all demonstrate lower melting enthalpies and crystallinities, which can explain their enhanced ionic conductivity. It is worth noting that the dissociation of $LiClO_4$ or $NaClO_4$ is an important factor improving the ionic conductivity. Hence, Fourier transform infrared (FTIR) spectroscopy was conducted to test the dissociation of $LiClO_4$ or $NaClO_4$. The peaks located at 624 and 635 cm^{-1} are attributed to the dissociated "free" ClO_{4-} ions and ion pairs $LiClO_4$/$NaClO_4$.[44] As shown in Fig. 6a and b, the dissociation of $LiClO_4$ in the PEO–Li and PEO–Na electrolytes is 95.2% and 95.4%, respectively, which is lower than that of PEO–7FDE–Li (97.6%) and PEO–5FDE–Na (97.5%), implying that the FDE filler composite polymer electrolyte can improve the dissociation of the electrolyte salt.

Based on the above-mentioned results, a schematic of the mechanism of FDE boosting the ionic conductivity was proposed, which is plotted in Fig. 7. Without the addition of FDE, the PEO electrolyte shows high crystallinity, which is not beneficial for the Li^+/Na^+ transport. There are a couple of positive influences that FDE can have on a composite electrolyte. First, the introduction of the FDE filler can effectively destroy the crystalline structure of the PEO polymer electrolyte, creating more amorphous regions. The polymer chain segment mobility is then enhanced, causing the rapid movement of Li^+/Na^+ in the electrolyte. Besides, FDE can adsorb/desorb Li^+/Na^+ on the surface, which could promote ion diffusion.

Besides the ionic conductivity, mechanical property is an important factor to evaluate the performance of a solid electrolyte.

To investigate the influence of the FDE filler on the mechanical property of polymer electrolytes, tensile strength testing was performed. As represented in Fig. 8a and b, the tensile strength of the PEO–7FDE–Li film can reach 1.71 MPa, while for PEO–Li, it is only 1.08 MPa. For PEO–5FDE–Na, the tensile strength increases as well (1.38 MPa) in comparison with the PEO–Na electrolyte (1.22 MPa). All the results indicated that the introduction of FDE can enhance the mechanical property of the composite electrolyte film. Moreover, as shown in Fig. S5 (ESI†), all the composite electrolyte films have good flexibility. After continuous folding and refolding, the electrolyte film can always recover to its initial appearance, indicating the potential to apply this composite electrolyte in flexible electronic devices. Electrochemical stability is important for ASSBs, especially for devices with high-voltage cathode materials. The composite electrolytes demonstrate enhanced electrochemical stability over the reference polymer electrolyte, and the curves are shown in Fig. 8c and d. It is observed that the PEO–7FDE–Li electrolyte has a stable electrochemical window up to 5 V, while an oxidative peak of the PEO–Li electrolyte appears at 4.6 V. In addition, the electrochemical window of the PEO–5FDE–Na electrolyte can reach 5 V, which has a significant improvement when compared with the PEO–Na electrolyte (3.5 V). Due to the addition of the FDE filler, the composite polymer electrolyte exhibits a wider electrochemical window, implying that the composite electrolyte can match well with high-voltage cathode materials.

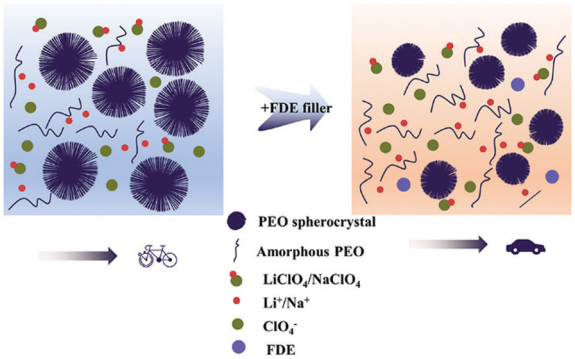

Fig. 7 Schematic of the mechanism for improving ionic conductivity.

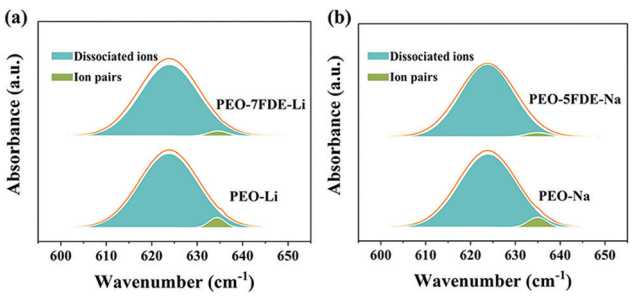

Fig. 6 . FTIR spectra of (a) PEO–Li, PEO–7FDE–Li and (b) PEO–Na, PEO–5FDE–Na at a wave number of 600–650 cm^{-1}.

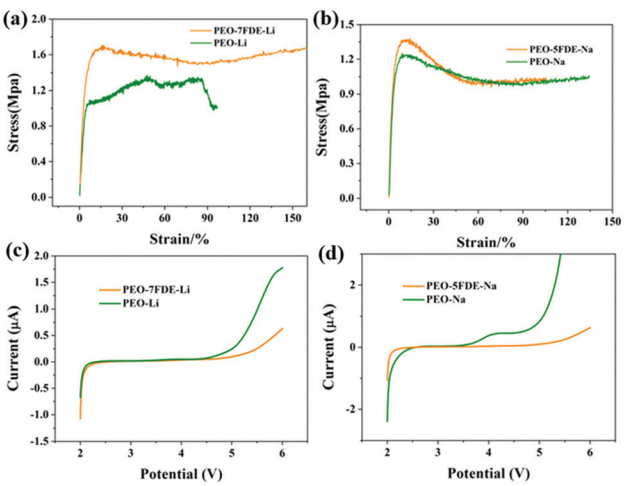

Fig. 8 Stress–strain curves of (a) PEO–Li and PEO–7FDE–Li and (b) PEO–Na and PEO–5FDE–Na. Electrochemical stability windows for (c) PEO–Li and PEO–7FDE–Li and (d) PEO–Na and PEO–5FDE–Na.

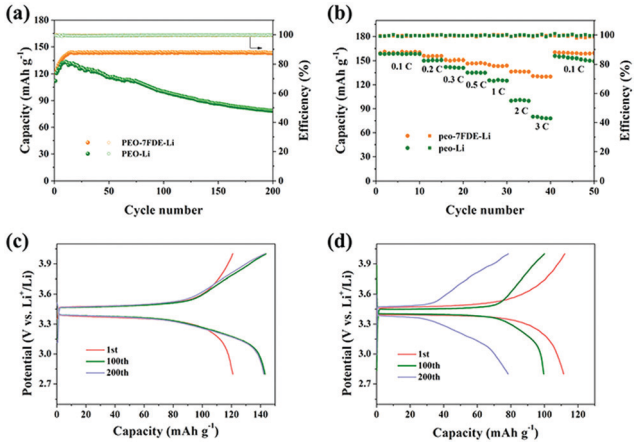

Fig. 9 Electrochemical performance of $LiFePO_4$/Li cells with PEO–7FDE–Li or PEO–Li as the electrolyte. (a) Cycling performance and coulombic efficiency at 1C rate between 2.5 V and 4.0 V *vs.* Li^+/Li. (b) Rate performance from 0.1C to 3C. Charge/discharge curves at different cycles for (c) PEO–7FDE–Li and (d) PEO–Li.

The investigations mentioned above can confirm that FDE is a promising filler. To further understand the effect of composite electrolytes on the electrochemical performance of a device, their corresponding batteries were assembled. Electrochemical measurement was performed at 1C (1C = 170.0 mA g^{-1}) at 60 °C, as plotted in Fig. 9a. The $LiFePO_4$/Li cell with the PEO–7FDE–Li electrolyte delivers an initial capacity of 121.0 mA h g^{-1}. Impressively, the reversible capacity is 142.8 mA h g^{-1} after 200 cycles, and during the cycling process, the coulombic efficiency reaches nearly 100%. Conversely, the capacity of the full cell based on the PEO–Li electrolyte shows a continuously declining trend and 78.5 mA h g^{-1} is retained after 200 cycles. The rate performances of the above-mentioned devices were also studied in detail (Fig. 9b). At a high rate of 3C, the $LiFePO_4$/Li cell with PEO–7FDE–Li electrolyte has a relatively high capacity of 139 mA h g^{-1}, which is much higher than that of the PEO–Li-based cell (77.9 mA h g^{-1}). At the same time, the capacity can recover to its original level when the current density is back to 0.1C, indicating a great rate retention of the capacity. All the results indicated the positive effect of the composite electrolyte on electrochemical performances. In addition to CE and rate performance, the polarization between the charging and the discharging platform, revealing the cycle stability, was studied to judge the comprehensive performance of a battery. As shown in the curves (Fig. 9c and d), it can be found that the polarization voltage first increased and then decreased for PEO–7FDE–Li and PEO–Li, implying the interface between the polymer electrolyte and the electrode is not stable at the very beginning. (The initial cycle is an interface activation process.) This trend of interface change is also reflected in the capacity of the cycle test (Fig. 9a). As shown in Fig. S6a (ESI†), the charge transfer resistance in the high-frequency semicircles displays the same trend, implying the activation process. Moreover, the PEO–7FDE–Li electrolyte-based cell displays a more stable polarization than the cell with the PEO–Li electrolyte, demonstrating the steady cycling performance of the PEO–7FDE–Li electrolyte.

Additionally, we studied the sodium-ion battery with composite electrolytes. Here, $Na_3V_2(PO_4)_3$ (NVP), as a promising cathode for sodium-ion batteries,[45] was applied in the device to assess the potential of the PEO–5FDE–Na and PEO–Na electrolytes in all-solid-state sodium-ion batteries. The full cell with $Na_3V_2(PO_4)_3$ as the cathode, Na metal as the anode, PEO–5FDE–Na as the electrolyte has an initial capacity of 49.2 mA h g^{-1} at 0.5C (1C = 117.6 mA g^{-1}). Moreover, the capacity can remain at 101.2 mA h g^{-1} after 100 cycles (Fig. 10a), while the capacity of the battery based on the PEO–Na electrolyte is much lower, which only delivers 67.5 mA h g^{-1} at 0.5C after 100 cycles (Fig. 10a). The rate performance and polarization voltage of the above-mentioned batteries are also discussed in detail. A high capacity of 74.0 mA h g^{-1} can be obtained from the battery based on the PEO–5FDE–Na electrolyte at a high rate of 3C, and impressively, the PEO–Na electrolyte-based cell shows no capacity (Fig. 10b). As plotted in Fig. 10c and d, the polarization voltage shows the same trend as that of the lithium-ion battery: first decreased and then increased. It can be found that the all-solid-state Na^+ battery also displays an interface activation process. The EIS trend shown in Fig. S6b (ESI†) demonstrates the same process. Note that the NVP/Na cell based on PEO–Na has a less stable polarization voltage than the corresponding PEO–5FDE–Na cell, demonstrating that cycling is more steady with the PEO–5FDE–Na electrolyte.

Since the interface between the polymer electrolyte and the electrode material is critical to the performance of the full cell, cycling tests of symmetric cells of Li|PEO–7FDE–Li|Li and Na|PEO–5FDE–Na|Na were conducted to investigate the interface (Fig. 11).[46,47] It is obvious that the polarization voltages of both samples show a gradually stabilizing process, in agreement with the previous cycling test results, and the curves indicate that both the overpotentials are stable after the activation process. The corresponding EIS tests were also conducted to confirm the trend (Fig. S7, ESI†). The resistance decreased

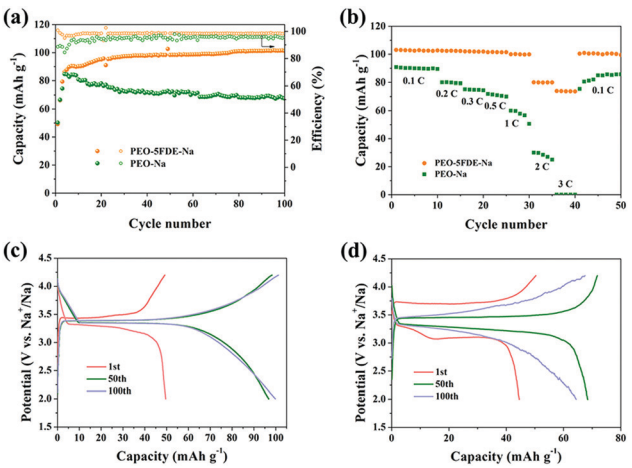

Fig. 10 Electrochemical performance of NVP/Na cells with PEO–Na or PEO–5FDE–Na as the electrolyte. (a) Cycling performance and coulombic efficiency at 0.5C between 2.0 V and 4.2 V *vs.* Na^+/Na. (b) Rate performance from 0.1C to 3C. Charge/discharge curves at different cycles for (c) PEO–5FDE–Na and (d) PEO–Na.

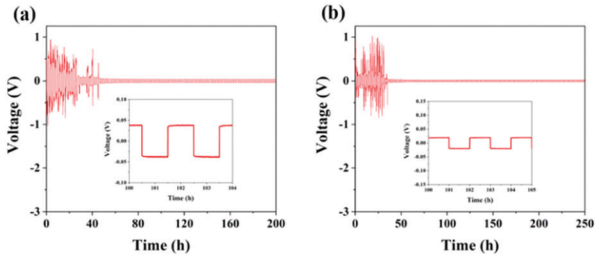

Fig. 11 Cycling performance for the symmetric cell (a) Li|PEO–7FDE–Li|Li and (b) Na|PEO–5FDE–Na|Na at a current density of 0.5 mA cm^{-2} at 60 °C. The insets are zoomed-in snapshots of the curves at certain time points.

during the initial cycling, indicating the activation process. The overpotential of the Li|PEO–7FDE–Li|Li cell remains stable for over 200 h at a current density of 0.5 mA cm^{-2}, and the Na symmetric cell with the PEO–5FDE–Na electrolyte has a steady overpotential within 250 h. The uniform plating and stripping of Li or Na in batteries based on PEO–7FDE–Li or PEO–5FDE–Na polymer electrolytes have a potential role in inhibiting the dendrite issues of Li and Na.

4. Conclusions

A sub-micron FDE filler has been fabricated by a facile eggshell conversion method with the assistance of ball-milling, and it was added with PEO to get a composite polymer electrolyte. In the composite electrolyte, the FDE filler can act as a Lewis base, relying on the Lewis acid–base interaction to combine the PEO polymer. The XRD results, microscope images and DSC data indicated that the crystallinity of PEO decreased and more amorphous regions were formed after the addition of the FDE filler, which is beneficial for Li^+/Na^+ transport. Compared with commercial CaO, the sub-micron size and multi-components of FDE cause a synergetic effect on improving the ionic conductivity of the electrolyte. Due to these advantages, composite polymer electrolytes of PEO–7FDE–Li and PEO–5FDE–Na exhibit ionic conductivities of 6.39×10^{-5} and 4.90×10^{-5} S cm^{-1} at room temperature, respectively, which are much higher than those of the PEO–Li (7.06×10^{-6} S cm^{-1}) and PEO–Na (6.10×10^{-6} S cm^{-1}) electrolytes. Furthermore, a stable cycling and excellent rate performance of the full cell based on the composite electrolyte were observed. The $LiFePO_4$/Li cell with the PEO–7FDE–Li electrolyte delivers a capacity of 142.8 mA h g^{-1} at 1C after 200 cycles. In addition, the $Na_3V_2(PO_4)_3$/Na battery based on the PEO–5FDE–Na electrolyte delivers a reversible capacity of 101.2 mA h g^{-1} at 0.5C after 100 cycles. The simple fabrication method and excellent electrochemical performance enable the FDE-based composite electrolyte extremely promising for ASSBs.

Conflicts of interest

There are no conflicts to declare.

Acknowledgements

This work was financially supported by National Key Research and Development Program of China (2019YFC1907805, 2018YFB0104200, 2018YFC1901605, and 2017YFB0102000), Hunan Provincial Science and Technology Plan (2017TP1001), Central South University Innovation Driven Project (2020CX007), and International Postdoctoral Exchange Fellowship Program (Talent-Introduction Program).

References

1 Y. Liang, C.-Z. Zhao, H. Yuan, Y. Chen, W. Zhang, J. Huang, D. Yu, Y. Liu, M.-M. Titirici, Y.-L. Chueh, H. Yu and Q. Zhang, A review of rechargeable batteries for portable electronic devices, *InfoMat*, 2019, **1**, 6–32.
2 L. Liu, H. Zhao and Y. Lei, Advances on three-dimensional electrodes for micro-supercapacitors: A mini-review, *InfoMat*, 2019, **1**, 74–84.
3 L. Xu, J. Li, Y. Li, P. Cai, C. Liu, G. Zou, H. Hou, L. Huang and X. Ji, Nitrogen-doped Carbon Coated $Na_3V_2(PO_4)_3$ with Superior Sodium Storage Capability, *Chem. Res. Chin. Univ.*, 2020, **36**, 459–466.
4 Z. Zeng, X. Liu, X. Jiang, Z. Liu, Z. Peng, X. Feng, W. Chen, D. Xia, X. Ai, H. Yang and Y. Cao, Enabling an intrinsically safe and high-energy-density 4.5 V-class Li-ion battery with nonflammable electrolyte, *InfoMat*, 2020, **2**, 984–992.
5 M. Yang, Z. Li, W. Chen, Y. Hu and Y. Yan, Carbon-Intercalated Montmorillonite as Efficient Polysulfide Mediator for Enhancing the Performance of Lithium–Sulfur Batteries, *Energy Fuels*, 2020, **34**, 8947–8955.
6 M. U. M. Patel and R. Dominko, Application of In Operando UV/Vis Spectroscopy in Lithium–Sulfur Batteries, *ChemSusChem*, 2014, **7**, 2167–2175.
7 R. Wang, M. Yao and Z. Niu, Smart supercapacitors from materials to devices, *InfoMat*, 2020, **2**, 113–125.
8 H. Li, L. Ren, D. Ai, Z. Han, Y. Liu, B. Yao and Q. Wang, Ternary polymer nanocomposites with concurrently enhanced dielectric constant and breakdown strength for high-temperature electrostatic capacitors, *InfoMat*, 2020, **2**, 389–400.
9 D. Li, L. Chen, T. Wang and L.-Z. Fan, 3D Fiber-Network-Reinforced Bicontinuous Composite Solid Electrolyte for Dendrite-free Lithium Metal Batteries, *ACS Appl. Mater. Interfaces*, 2018, **10**, 7069–7078.
10 H. Xie, C. Yang, K. K. Fu, Y. Yao, F. Jiang, E. Hitz, B. Liu, S. Wang and L. Hu, Flexible, Scalable, and Highly Conductive Garnet-Polymer Solid Electrolyte Templated by Bacterial Cellulose, *Adv. Energy Mater.*, 2018, **8**, 1703474.
11 L. Chen, Y. Li, S.-P. Li, L.-Z. Fan, C.-W. Nan and J. B. Goodenough, PEO/garnet composite electrolytes for solid-state lithium batteries: From ''ceramic-in-polymer'' to ''polymer-in-ceramic'', *Nano Energy*, 2018, **46**, 176–184.
12 L. Xu, J. Li, W. Deng, H. Shuai, S. Li, Z. Xu, J. Li, H. Hou, H. Peng, G. Zou and X. Ji, Garnet Solid Electrolyte for

Advanced All-Solid-State Li Batteries, *Adv. Energy Mater.*, 2020, DOI: 10.1002/aenm.202000648.

13 C. Zhao, Y. Lu, L. Chen and Y.-S. Hu, Flexible Na batteries, *InfoMat*, 2020, **2**, 126–138.

14 J. Wan, J. Xie, X. Kong, Z. Liu, K. Liu, F. Shi, A. Pei, H. Chen, W. Chen, J. Chen, X. Zhang, L. Zong, J. Wang, L. Q. Chen, J. Qin and Y. Cui, Ultrathin, flexible, solid polymer composite electrolyte enabled with aligned nanoporous host for lithium batteries, *Nat. Nanotechnol.*, 2019, **14**, 705–711.

15 T. Ates, M. Keller, J. Kulisch, T. Adermann and S. Passerini, Development of an all-solid-state lithium battery by slurry-coating procedures using a sulfidic electrolyte, *Energy Storage Mater.*, 2019, **17**, 204–210.

16 X. Han, Y. Gong, K. K. Fu, X. He, G. T. Hitz, J. Dai, A. Pearse, B. Liu, H. Wang, G. Rubloff, Y. Mo, V. Thangadurai, E. D. Wachsman and L. Hu, Negating interfacial impedance in garnet-based solid-state Li metal batteries, *Nat. Mater.*, 2017, **16**, 572–579.

17 A. L. Ahmad, U. R. Farooqui and N. A. Hamid, Synthesis and characterization of porous poly(vinylidene fluoride-*co*-hexafluoro propylene) (PVDF-*co*-HFP)/poly(aniline) (PANI)/graphene oxide (GO) ternary hybrid polymer electrolyte membrane, *Electrochim. Acta*, 2018, **283**, 842–849.

18 N. Zhao, W. Khokhar, Z. Bi, C. Shi, X. Guo, L.-Z. Fan and C.-W. Nan, Solid Garnet Batteries, *Joule*, 2019, **3**, 1190–1199.

19 L. Long, S. Wang, M. Xiao and Y. Meng, Polymer electrolytes for lithium polymer batteries, *J. Mater. Chem. A*, 2016, **4**, 10038–10069.

20 A. Manthiram, X. Yu and S. Wang, Lithium battery chemistries enabled by solid-state electrolytes, *Nat. Rev. Mater.*, 2017, **2**, 16103.

21 C. Wang, T. Wang, L. Wang, Z. Hu, Z. Cui, J. Li, S. Dong, X. Zhou and G. Cui, Differentiated Lithium Salt Design for Multilayered PEO Electrolyte Enables a High-Voltage Solid-State Lithium Metal Battery, *Adv. Sci.*, 2019, **6**, 1901036.

22 Z. Li, H.-M. Huang, J.-K. Zhu, J.-F. Wu, H. Yang, L. Wei and X. Guo, Ionic Conduction in Composite Polymer Electrolytes: Case of PEO:Ga-LLZO Composites, *ACS Appl. Mater. Interfaces*, 2019, **11**, 784–791.

23 N. Molinari, J. P. Mailoa and B. Kozinsky, Effect of Salt Concentration on Ion Clustering and Transport in Polymer Solid Electrolytes: A Molecular Dynamics Study of PEO–LiTFSI, *Chem. Mater.*, 2018, **30**, 6298–6306.

24 X. Yu, L. Xue, J. B. Goodenough and A. Manthiram, Ambient-Temperature All-Solid-State Sodium Batteries with a Laminated Composite Electrolyte, *Adv. Funct. Mater.*, 2020, DOI: 10.1002/adfm.202002144.

25 P. Yao, B. Zhu, H. Zhai, X. Liao, Y. Zhu, W. Xu, Q. Cheng, C. Jayyosi, Z. Li, J. Zhu, K. M. Myers, X. Chen and Y. Yang, PVDF/Palygorskite Nanowire Composite Electrolyte for 4 V Rechargeable Lithium Batteries with High Energy Density, *Nano Lett.*, 2018, **18**, 6113–6120.

26 P. Pal and A. Ghosh, Investigation of ionic conductivity and relaxation in plasticized PMMA–$LiClO_4$ solid polymer electrolytes, *Solid State Ionics*, 2018, **319**, 117–124.

27 Y. Zhu, J. Cao, H. Chen, Q. Yu and B. Li, High electrochemical stability of a 3D cross-linked network PEO@nano-SiO_2 composite polymer electrolyte for lithium metal batteries, *J. Mater. Chem. A*, 2019, **7**, 6832–6839.

28 N. Zhang, J. He, W. Han and Y. Wang, Composite solid electrolyte PEO/SN/$LiAlO_2$ for a solid-state lithium battery, *J. Mater. Sci.*, 2019, **54**, 9603–9612.

29 A. Lassagne, E. Beaudoin, A. Ferrand, T. N. T. Phan, P. Davidson, C. Iojoiu and R. Bouchet, New approach to design solid block copolymer electrolytes for 40 °C lithium metal battery operation, *Electrochim. Acta*, 2017, **238**, 21–29.

30 J. Shim, D.-G. Kim, H. J. Kim, J. H. Lee, J.-H. Baik and J.-C. Lee, Novel composite polymer electrolytes containing poly(ethylene glycol)-grafted graphene oxide for all-solid-state lithium-ion battery applications, *J. Mater. Chem. A*, 2014, **2**, 13873–13883.

31 A. C. Nancy and S. A. Suthanthiraraj, Effect of Al_2O_3 nanofiller on the electrical, thermal and structural properties of PEO:PPG based nanocomposite polymer electrolyte, *Ionics*, 2017, **23**, 1439–1449.

32 D. Lin, W. Liu, Y. Liu, H. R. Lee, P.-C. Hsu, K. Liu and Y. Cui, High Ionic Conductivity of Composite Solid Polymer Electrolyte *via In Situ* Synthesis of Monodispersed SiO_2 Nanospheres in Poly(ethylene oxide), *Nano Lett.*, 2016, **16**, 459–465.

33 P. Dhatarwal and R. J. Sengwa, Dielectric relaxation, Li-ion transport, electrochemical, and structural behaviour of PEO/PVDF/$LiClO_4$/TiO_2/PC-based plasticized nanocomposite solid polymer electrolyte films, *Compos. Commun.*, 2020, **17**, 182–191.

34 T. Dam, S. N. Tripathy, M. Paluch, S. S. Jena and D. K. Pradhan, Investigations of Relaxation Dynamics and Observation of Nearly Constant Loss Phenomena in PEO_{20}–$LiCF_3SO_3$–ZrO_2 Based Polymer Nano-Composite Electrolyte, *Electrochim. Acta*, 2016, **202**, 147–156.

35 W. Tang, S. Tang, X. Guan, X. Zhang, Q. Xiang and J. Luo, High-Performance Solid Polymer Electrolytes Filled with Vertically Aligned 2D Materials, *Adv. Funct. Mater.*, 2019, **29**, 1900648.

36 Y. Li, Z. Sun, D. Liu, Y. Gao, Y. Wang, H. Bu, M. Li, Y. Zhang, G. Gao and S. Ding, A composite solid polymer electrolyte incorporating MnO_2 nanosheets with reinforced mechanical properties and electrochemical stability for lithium metal batteries, *J. Mater. Chem. A*, 2020, **8**, 2021–2032.

37 C. Ma, K. Dai, H. Hou, X. Ji, L. Chen, D. G. Ivey and W. Wei, High Ion-Conducting Solid-State Composite Electrolytes with Carbon Quantum Dot Nanofillers, *Adv. Sci.*, 2018, **5**, 1700996.

38 B. Kumar, S. Nellutla, J. S. Thokchom and C. Chen, Ionic conduction through heterogeneous solids: Delineation of the blocking and space charge effects, *J. Power Sources*, 2006, **160**, 1329–1335.

39 P. J. Alarco, Y. Abu-Lebdeh, A. Abouimrane and M. Armand, The plastic-crystalline phase of succinonitrile as a universal matrix for solid-state ionic conductors, *Nat. Mater.*, 2004, **3**, 476–481.

40 J. Zhang, N. Zhao, M. Zhang, Y. Li, P. K. Chu, X. Guo, Z. Di, X. Wang and H. Li, Flexible and ion-conducting membrane electrolytes for solid-state lithium batteries: Dispersion of garnet nanoparticles in insulating polyethylene oxide, *Nano Energy*, 2016, **28**, 447–454.

41 X. Xu, H. Wang, L. Jiang, X. Wang, S. A. Payne, J. Y. Zhu and R. Li, Comparison between Cellulose Nanocrystal and Cellulose Nanofibril Reinforced Poly(ethylene oxide) Nanofibers and Their Novel Shish-Kebab-Like Crystalline Structures, *Macromolecules*, 2014, **47**, 3409–3416.

42 T. Caruso, S. Capoleoni, E. Cazzanelli, R. G. Agostino, P. Villano and S. Passerini, Characterization of PEO-lithium triflate polymer electrolytes: Conductivity, DSC and Raman Investigations, *Ionics*, 2002, **8**, 36–43.

43 Y. Tong, L. Chen, X. He and Y. Chen, Free Mesogen Assisted Assembly of the Star-shaped Liquid-crystalline Copolymer/Polyethylene Oxide Solid Electrolytes for Lithium Ion Batteries, *Electrochim. Acta*, 2014, **118**, 33–40.

44 M. Salomon, M. Xu, E. D. Eyring and S. Petrucci, Molecular Structure and Dynamics of $LiClO_4$-Polyethylene Oxide-400 (Dimethyl Ether and Diglycol Systems) at 25 °C, *J. Phys. Chem.*, 1994, **98**, 8234–8244.

45 J. Cao, Y. Wang, L. Wang, F. Yu and J. Ma, $Na_3V_2(PO_4)_3$@C as faradaic Electrodes in Capacitive Deionization for High-Performance Desalination, *Nano Lett.*, 2019, **19**, 823–828.

46 W. Chen, Y. Hu, W. Lv, T. Lei, X. Wang, Z. Li, M. Zhang, J. Huang, X. Du, Y. Yan, W. He, C. Liu, M. Liao, W. Zhang, J. Xiong and C. Yan, Lithiophilic montmorillonite serves as lithium ion reservoir to facilitate uniform lithium deposition, *Nat. Commun.*, 2019, **10**, 4973.

47 Y. Hu, W. Chen, T. Lei, Y. Jiao, H. Wang, X. Wang, G. Rao, X. Wang, B. Chen and J. Xiong, Graphene quantum dots as the nucleation sites and interfacial regulator to suppress lithium dendrites for high-loading lithium-sulfur battery, *Nano Energy*, 2020, **68**, 104373.

48 J. Li, H. Wei, Y. Peng, L. Geng, L. Zhu, X.-Y. Cao, C.-S. Liu and H. Pang, A multifunctional self-healing G-PyB/KCl hydrogel: smart conductive, rapid room-temperature phase-selective gelation, and ultrasensitive detection of alpha-fetoprotein, *Chem. Commun.*, 2019, **55**, 7922–7925.